ASCE

Quantification of Urban Resilience to Natural Hazards from Traffic-Flow Data

Georgios Chatzikyriakidis, S.M.ASCE[1]; Nicos Makris, F.ASCE[2]; and Tue Vu, S.M.ASCE[3]

Abstract: Given that in addition to the robustness of the transportation, utility, electricity, and telecommunication networks, perhaps the most robust network that serves urban resilience is the living network of the citizens of a city, in this paper we quantify urban resilience to natural hazards by processing traffic-flow data. From the recorded traffic-flow values (number of vehicles per time) at various locations on major traffic city arteries, we compute the probability density for finding a vehicle at some distance x, from the city center at time t, and, subsequently, we calculate the time history of the mean-square displacement (MSD) of vehicles from the city center. The shape of the MSD time histories computed in this study from traffic-flow data exhibits striking similarities with the MSD time histories computed by tracking GPS locations from individual cellphone users. Accordingly, this study that uses an entirely different type of data confirms our previous finding that large American cities, following a natural hazard, revert immediately to their initial steady-state behavior and resume their normal, pre-event activities. **DOI:** 10.1061/JENMDT.EMENG-8724. *© 2025 American Society of Civil Engineers.*

Introduction

The functionality of cities is the outcome of the superposition of complex networks including the transportation infrastructure (roads, bus lines, and a subway network when available), water and gas utility networks, the electricity grid, and telecommunication networks (telephone and Internet) together with overriding social networks (Bettencourt 2013; Lhomme et al. 2013; Cruz et al. 2013; Cassottana et al. 2019; Blagojević et al. 2023). Fig. 1 shows schematically the superposition of the various aforementioned infrastructure networks for the Dallas metroplex in Texas. All of these complex networks have been created and upgraded independently at different times with no apparent common design principles. In addition to these aforementioned material, electricity, and electronic networks, perhaps the most robust network that serves urban resilience is the living network of the citizens since cities are essentially the physical manifestation of the daily interactions of its citizens facilitating the generation of creativity, growth, progress, and leadership together with economic, intellectual, and social wealth. Various definitions of the term resilience in association with proposed metrics have been proposed in the literature (Bruneau et al. 2003; Godschalk2003; Da Silva et al. 2012; Jabareen 2013; Meerow et al. 2016) testifying to the richness of the concept while presenting challenges associated with its quantification (Henry and Ramirez-Marquez 2012; Linkov et al. 2014; Ganin et al. 2016). Our definition of *urban resilience* adopted in this study is rooted in the seminal work of Holling (1973, 1996), who distinguished *engineering resilience* from *ecological resilience*. The more traditional definition associated with *engineering resilience* hinges upon the ability of a system to *assume stable equilibrium* (or steady-state regime at equilibrium), and, in this case, resilience is defined as the capacity of the system, following a disturbance (shock), to recover its initial equilibrium state and revert to its normal, pre-event activity. The second definition associated with *ecological resilience* emphasizes conditions *far from equilibrium* where instabilities can flip a system into another regime of behavior—that is, a different equilibrium state. In this case, resilience is associated with the magnitude of a disturbance (shock) that needs to be absorbed by the system before it changes its structure and stabilizes at a different equilibrium state (Holling 1996). In this work, which builds upon our past study, Makris et al. (2023a, b), *urban resilience to natural hazards* is defined as the ability of a large city, following a natural hazard, to revert to its initial steady-state behavior and resume its normal, pre-event activities—a definition that matches Holling's (1996) definition of engineering resilience.

Motivated from the need to encode into the resilience of a city the resilience of the living network of its citizens (Bettencourt and West 2010; Bettencourt 2013), Makris et al. (2023a, b) selected as a metric, which represents the response of a city during and away from equilibrium, the mean-square displacement (MSD) $\langle r^2(t)\rangle$ of its citizens, where $r(t)$ is the distance of a citizen (cellphone ID) from its home at time t

$$\langle r^2(t)\rangle = \frac{1}{M}\sum_{j=1}^{M} r_j^2(t) = \frac{1}{M}\sum_{j=1}^{M}\left(x_j^2(t) + y_j^2(t)\right) \tag{1}$$

and M is the number of an ensemble of citizens (IDs) in the city that we are examining.

Accordingly, our earlier studies adopted a GPS location tracking approach of cellphone IDs as indicated by Eq. (1), in a similar way that particle tracking is achieved in microrheology with dynamic light scattering (Mason and Weitz 1995; Mason et al. 1997; Palmer et al. 1998; Schnurr et al. 1997; Li et al. 2010; Li and Raizen 2013) or with laser interferometry (Schnurr et al. 1997; Gittes et al. 1997). Our past framework of analysis concentrated on a *single-state equilibrium*, which is the *response history of the mean-square displacement* of the citizens from their individual homes of the entire city when it operates under normal conditions—a response

[1]Ph.D. Student, Dept. of Civil and Environmental Engineering, Southern Methodist Univ., Dallas, TX 75205. ORCID: https://orcid.org/0009-0003-6347-5361. Email: gchatzikyriakidis@mail.smu.edu

[2]Professor, Dept. of Civil and Environmental Engineering, Southern Methodist Univ., Dallas, TX 75205 (corresponding author). ORCID: https://orcid.org/0000-0002-9059-2147. Email: nmakris@mail.smu.edu

[3]Research Scientist, Research Technology Services, Office of Information Technology, Southern Methodist Univ., Dallas, TX 75275-0480. Email: tuev@mail.smu.edu

Note. This manuscript was submitted on June 30, 2025; approved on September 3, 2025; published online on December 5, 2025. Discussion period open until May 5, 2026; separate discussions must be submitted for individual papers. This paper is part of the ***Journal of Engineering Mechanics***, © ASCE, ISSN 0733-9399.

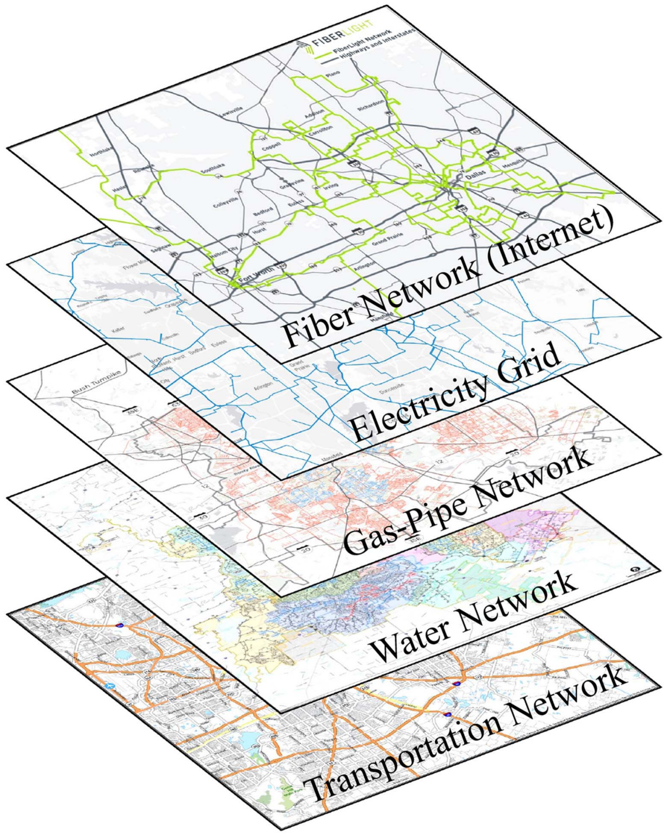

Fig. 1. Transportation, utility, and telecommunication infrastructure networks of the Dallas metroplex that have been created and upgraded independently during different times with no apparent common design principles. The superposition of these independent infrastructure networks creates a difficult-to-interpret "redundancy" that apparently serves urban resilience. (Reprinted from Makris et al. 2023b, © ASCE.)

parameter that captures with fidelity the physical manifestation of the daily interactions of the citizens of a large city through their collective mobility patterns. In the language of continuum mechanics, this particle tracking approach resembles a Lagrangian formulation in solid mechanics. Our past studies examined (1) the response of the Dallas and Houston metroplexes that were subjected to the February 2021 North American winter storm (Makris et al. 2023a, b); and (2) the response of three large US cities (Houston, Miami, and Jacksonville) when subjected to Category 4 and 5 hurricanes (2017 Harvey, 2017 Irma, and 2019 Dorian); Makris et al. (2023b) and revealed that the MSD $= \langle r^2(t) \rangle$ as computed by tracking cellphone IDs of all the aforementioned cities when subjected to the corresponding violent natural hazard reverts immediately to its pre-event pattern upon the expiration of the duration of the natural hazard.

As an example Fig. 2 plots the time histories of the MSD $= \langle r^2(t) \rangle$ from the homes of the citizens of the ensembles distilled during the first quarter of 2021 for the city of Dallas [Fig. 2(a)] and the city of Houston [Fig. 2(b)] (Makris et al. 2023b). Fig. 2 reveals that while the MSDs for the Dallas and Houston greater urban areas exhibit a stable daily and weekly periodicity, they exhibit a noticeable suppression during the duration of the North American winter storm. What is remarkable in Fig. 2 is that immediately after the expiration of the cold winter storm (sometime by Saturday, February 20, 2021) (National Oceanic and Atmospheric Administration 2021; National Weather Service 2021), both the city of Dallas and the city of Houston resume normal activity with the MSD of its citizens to revert back to its normal oscillation pattern as recorded prior to the storm. This invariant, systematic ability of large American cities, following a natural hazard, to revert immediately to their initial steady-state behavior and resume their normal, pre-event activities suggests that large American cities, at the system-wide scale, exhibit a high degree of inherent resilience to natural hazards; see also Makris et al. (2023b). This large degree of *engineering* resilience was also uncovered for local communities within the large urban centers (Chatzikyriakidis et al. 2026) where the distilled cellphone IDs are these that their homes are in the identified community of interest.

Fig. 2 shows that the mean value of the MSD for the Dallas metroplex as computed upon tracking cellphone GPS location data is $A_0 = 165\ \text{km}^2$, whereas the mean value of the MSD for Houston is $A_0 = 80\ \text{km}^2$. While the mean value of the MSD is a measure of the mobility of the citizens in a given urban center, our analysis methodology hinges only upon the normalized expressions of these MSD time histories and not on their magnitude values, since we are

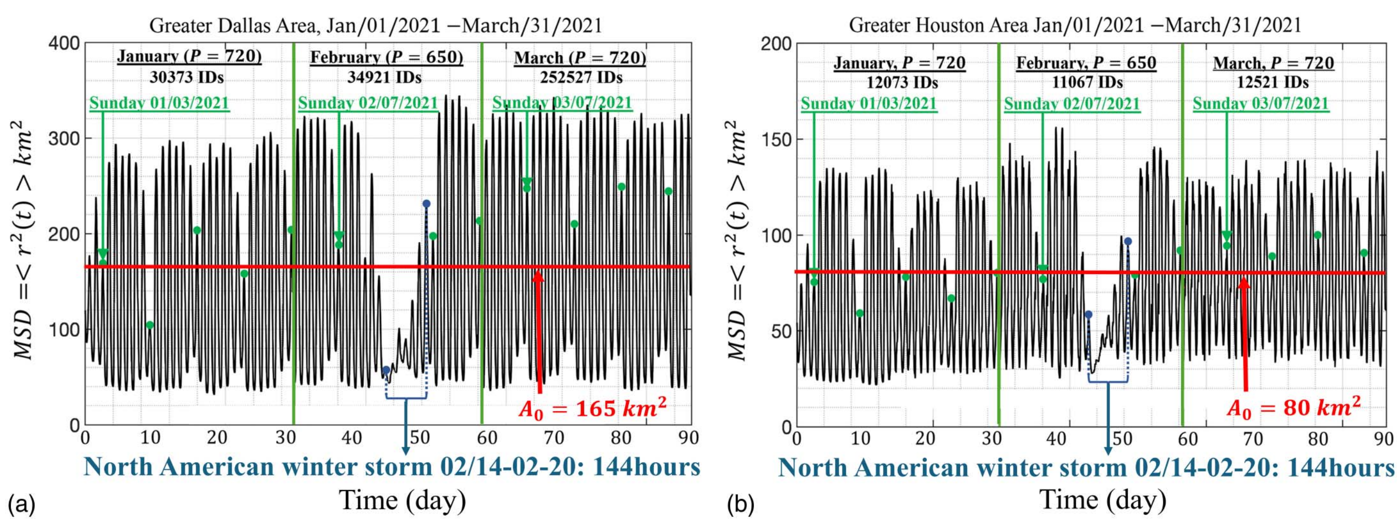

Fig. 2. Time history of the mean-square displacement $\langle r^2(t) \rangle$ (ensemble average) of cellphone IDs in (a) Dallas metroplex; and (b) city of Houston during $Q1$ of 2021. Dots atop the suppressed spikes indicate Sundays.

primarily interested in extracting the recovery time of a city upon being struck from a natural hazard.

In an effort to reinforce our past findings regarding the inherent resilience of large American cities to natural hazards, as shown in Fig. 2, in this paper we quantify urban resilience by processing an entirely different set of data, that is, traffic-flow data. In this study we process traffic-flow data on selective traffic city arteries that go through the cities of Dallas and Houston that were made available by the TxDOT, North Central Texas Council of Governments, and Texas A&M Transportation Institute, respectively (North Central Texas Council of Governments 2025; Texas A&M Transportation Institute 2025), and we compute the mean-square displacement of vehicles from the centers of the Cities of Dallas and Houston. In the language of continuum mechanics, monitoring traffic-flow data resembles an Eulerian formulation in fluid mechanics. The traffic-flow histories (Eulerian approach) used in this study are nearly identical to the mean-square displacement histories $\langle r^2(t)\rangle$ computed from tracking cellphone IDs (Lagrangian approach) given by Eq. (1) and shown in Fig. 2. In this paper we explain the reason for this striking similarity, while the structure of the mean-square displacements of vehicles from a city center computed from traffic-flow data reinforces our past conclusions (Makris et al. 2023a, b) regarding an inherent resilience of large American cities to natural hazards.

Time Histories of Total Number of Vehicles Moving along Traffic City Arteries

State Departments of Transportations, such as TxDOT North Central Texas Council of Governments and the Texas A&M Transportation Institute (North Central Texas Council of Governments 2025; Texas A&M Transportation Institute 2025), monitor the traffic-flow of vehicles along major traffic city arteries that go through cities by measuring the number of vehicles per time (traffic-flow = Q) that go across various sections of the traffic arteries (Dalziell and Nicholson 2001; Min and Wynter 2011; Jindal et al. 2013; Shi and Abdel-Aty 2015; Roh et al. 2016; Achillopoulou et al. 2020; Qiang and Xu 2020; Yuan and Li 2021). As an example, Fig. 3(a) shows the location of six monitoring stations ($M = 6$) along freeway I-30, together with the locations of six monitoring stations ($M = 6$) along freeway I-35E that essentially pass through the center of Dallas, TX. Fig. 3(b) shows many more locations of monitoring stations along freeways I-10 and I-45 together with US highways 288 and 290, which essentially pass through the center of Houston.

We are interested in calculating the mean-square displacement $\langle x^2(t)\rangle$ of the vehicles along a given freeway from the center of the city within the limits of the greater urban area at any given time t. In the interest of simplicity we assume that the freeways of interest that go through the city are straight lines so that we can proceed with a one-dimensional analysis. As an example, Fig. 4(a) shows the locations of the monitoring stations where traffic-flow is measured along freeway I-30 as traffic-flow moves from west to east; meanwhile, Fig. 4(b) shows the corresponding measuring location as traffic-flow moves from east to west. The stations measuring the eastbound and westbound traffic are a few meters apart along the freeway, yet for the engineering accuracy of this study, they are assumed at the same location as shown in Fig. 4.

In Figs. 5(a and b) show the time histories of the number of vehicles per minute (traffic-flow = Q_2 with units $[T]^{-1}$) that crosses the second station from west of freeway I-30. Plot (a) is for eastbound traffic (station 672), whereas plot (b) is for westbound traffic (station 619). Figs. 5(c and d) plot the traffic-flow Q_2 = (number of vehicles)/minute that crosses the second station from the south of freeway I-35E, during the first quarter of year 2021. Plot (c) is for northbound traffic (station 782), whereas plot (d) is for southbound traffic (stations 783). What is remarkable about the traffic-flow histories shown in Fig. 5 is their striking similarity with the mean-square displacement histories of an ensemble of citizens (cellphone IDs) from their homes shown in Fig. 2.

Assuming that the velocity of a vehicle that crosses section $j \in \{1, 2, \ldots, M\}$ is v_j, and that the vehicles are moving on an average at a constant speed, then the time t_j needed for a vehicle to run the segment S_j, which spans the mid-distance from station $j-1$ to station j up to the mid-distance from station j to station $j+1$, is

$$t_j = \frac{S_j}{v_j(t)} \tag{2}$$

Consequently, with reference to Fig. 4, at any time t, the number of vehicles, $N_j(t)$, that happen to be along the segment S_j is

$$N_j(t) = Q_j(t) \cdot t_j = Q_j(t) \cdot \frac{S_j}{v_j(t)} \tag{3}$$

which is a dimensionless number: $[N_j(t)] = [T]^{-1}[L][L]^{-1}[T] = [1]$.

The number of vehicles that happen to be moving at time t along the eastbound lanes as they move from the west outskirts of the city, say L_W, to the east outskirts of the city, L_E, is

$$\sum_{j=1}^{M^{E-W}} N_j^E(t) = \sum_{j=1}^{M^{E-W}} Q_j^E(t)\frac{S_j}{v_j^E(t)} \tag{4}$$

where the superscript E = eastbound traffic; and the number of segments M is labeled as M^{E-W} for the specific freeway. For I-35E, which runs north–south, the number of segments will be labeled M^{N-S}.

Similarly, the number of vehicles that happen to be moving at time t along a given freeway on the westbound lanes as they move from L_E to L_W is

$$\sum_{j=1}^{M^{E-W}} N_j^W(t) = \sum_{j=1}^{M^{E-W}} Q_j^W(t)\frac{S_j}{v_j^W(t)} \tag{5}$$

where the superscript W = westbound traffic.

Accordingly, the total number of vehicles $N^{E-W}(t)$ that are moving along a E-W freeway at time t within the limits of interest (say from L_W to L_E) is

$$N^{E-W}(t) = \sum_{j=1}^{M^{E-W}} (N_j^E(t) + N_j^W(t)) = \sum_{j=1}^{M^{E-W}} \left(\frac{Q_j^E(t)}{v_j^E(t)} + \frac{Q_j^W(t)}{v_j^W(t)}\right) S_j \tag{6}$$

Fig. 6 plots the time histories of the total number of vehicles $N^{E-W}(t)$ that happen to be moving along freeway I-30 between the segment $L_W - L_E = 21.26$ km [Fig. 6(a)] and $N^{N-S}(t)$ that happen to be moving along freeway I-35E between the segment $L_S - L_N = 19.95$ km [Fig. 6(b)], during the first quarter of 2021. The total number of vehicle time histories, $N^{E-W}(t)$ and $N^{N-S}(t)$ shown in Fig. 6, manifest a striking similarity to the time histories of the MSD of an ensemble of citizens (cellphone IDs) from their homes as shown in Fig. 2. Again, Fig. 6 reveals that immediately after the expiration of the cold winter storm, the activity of the city of Dallas as encoded with the traffic-flow data along two main traffic city arteries, freeways I-30 and I-35E, resumes its normal regime with the total number of vehicles on each of the two freeways to revert back to the normal oscillation patterns as recorded prior to the winter storm.

J. Eng. Mech., 2026, 152(2): 04025098

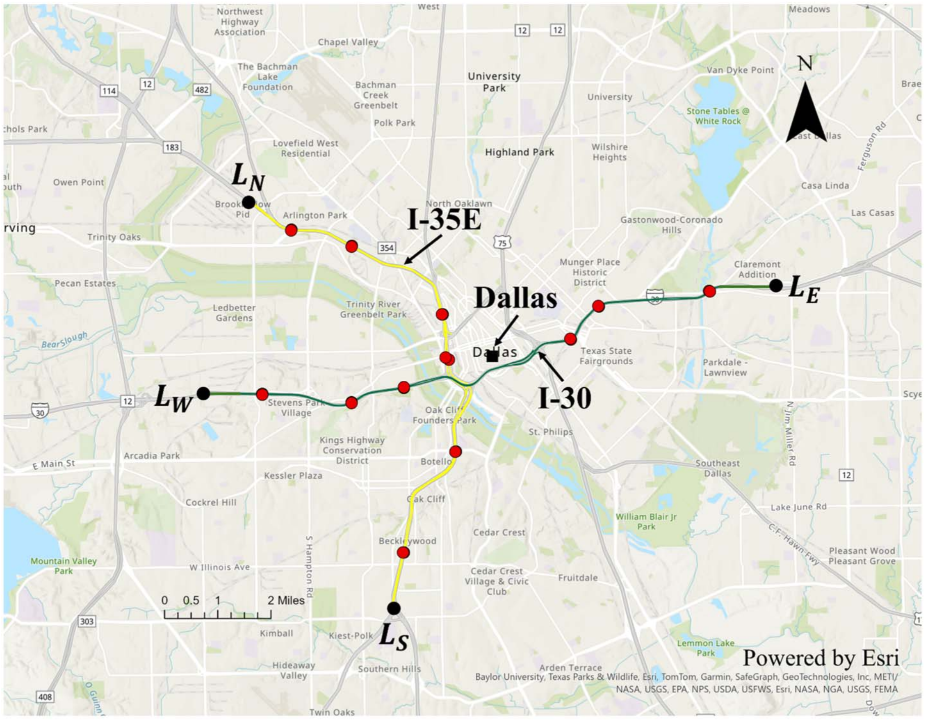

(a)

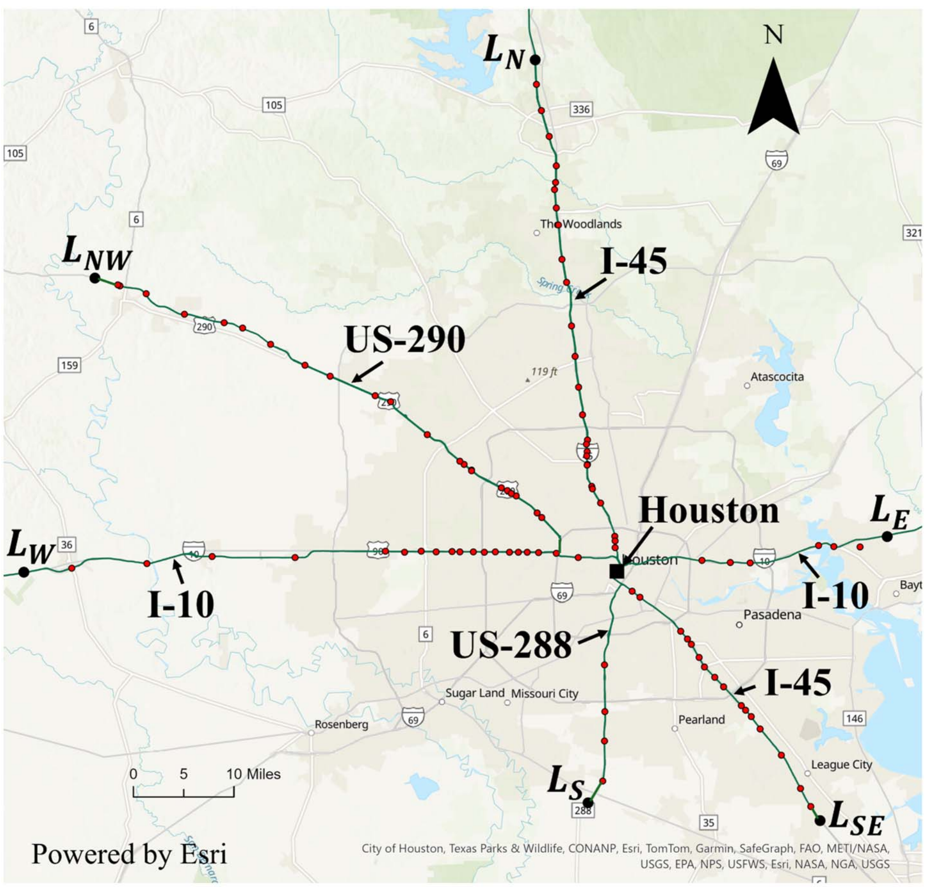

(b)

Fig. 3. (a) Locations of monitoring stations (dots) of traffic-flow Q = (number of vehicles)/time along freeway I-30 and I-35E that pass through the center of the city of Dallas, TX. (b) Locations of monitoring stations (dots) of traffic-flow Q = (number of vehicles)/time along freeways I-10 and I-45 and highways US-288 and US-290 that pass through the center of the city of Houston, TX. [Map data (a) from ArcGIS World Topographic Map, Sources: Baylor University, Texas Parks & Wildlife, Esri, TomTom, Garmin, SafeGraph, GeoTechnologies, Inc., METI/NASA, USGS, EPA, NPS, USDA, USFWS, Esri, NASA, NGA, USGS, FEMA; (b) from ArcGIS World Topographic Map, Sources: City of Houston, Texas Parks & Wildlife, CONANP, Esri, TomTom, Garmin, SafeGraph, FAO, METI/NASA, USGS, EPA, NPS, USFWS, Esri, NASA, NGA, USGS.]

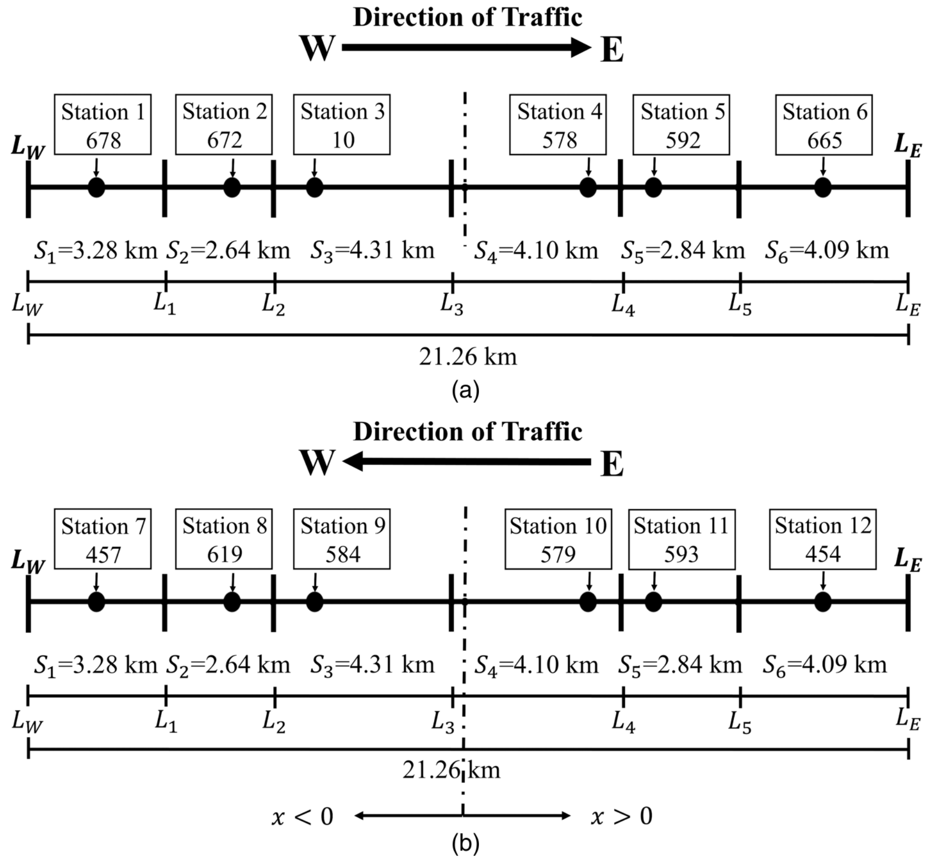

Fig. 4. Locations of the stations that measure traffic-flow Q = (number of vehicles)/time together with the distances from mid-distance to mid-distance of these stations (west–east). The locations of L_W and L_E are arbitrary—in this case the location is such that the first and last stations are at mid-distance of segments S_1 and S_6.

Up to this point, our study concludes that in addition to the mean-square displacement metric $\langle r^2(t)\rangle$ that was used to quantify urban resilience to natural hazards (Makris et al. 2023a, b) one can use an alternative metric, that is, the number of vehicles moving on major traffic city arteries, $N^{E-W}(t)$, or $N^{N-S}(t)$, or even $N(t) = \sum_{\alpha=1}^{A} N^{\alpha}(t)$, where A is the total number of traffic city arteries that pass through the center of a city and $N^{\alpha}(t)$ is the total number of vehicles that happen to be moving along freeway α, as shown in Fig. 6, which uncovers the same main conclusion. Our study proceeds one step further by using the traffic-flow data shown in Fig. 5 to compute mean-square displacement histories $\langle x^2(t)\rangle$ of the vehicles moving along these major city arteries from the city center.

From Traffic-Flow Data to a Mean-Square Displacement of Vehicles from the City Center

Our interest to build an expression of a mean-square displacement of an ensemble of vehicles that move along major traffic city arteries from traffic-flow data is motivated from the need to relate human mobility data to a physics-based model. Since Einstein's 1905 seminal paper (1905) on the quantitative theory of Brownian motion, which presented for the first time the long-term relation (diffusive regime) between the mean-square displacement of Brownian particles, $\langle r^2(t)\rangle$, and the diffusion coefficient of the fluid, $D(\langle r^2(t)\rangle = 2Dt)$, there has been a growing interest in this physical process given that the equation that describes the motion of a Brownian particle immersed in some liquid that is in thermal equilibrium applies to a wide range of stochastic (random) processes from which deterministic time-response functions emerge when the system is at a steady-state equilibrium (Mason and Weitz 1995; Attard 2012; Li and Raizen 2013; Coffey and Kalmykov 2012; Makris 2020, 2021a, b).

It so happens that regardless of the complexity of the mechanism that the immersed Brownian particles exchange forces with the surrounding isotropic fluid (viscous, inertia, hydrodynamic memory or viscoelastic forces) (Ornstein 1917; Uhlenbeck and Ornstein 1930; Wang and Uhlenbeck 1945; Mason and Weitz 1995; Makris 2020, 2021b), the mean-square displacement of a collection of Brownian particles, $\langle r^2(t)\rangle$, which is an ensemble average from a stochastic (random) process, is proportional to a deterministic time-response function that is the creep compliance $J(t)$ (strain history due to a unit-step stress) of a mechanical model

$$\langle r^2(t)\rangle = WJ(t) \tag{7}$$

In view of the overarching validity of Eq. (7), Makris et al. (2023a, b) built upon the profound implications of Eq. (7) to conjecture a corresponding relation for cities. Accordingly in this section we proceed by computing the mean-square displacement of the vehicles along major traffic city arteries from the city center as computed from traffic-flow data and compare its form (oscillating pattern) with the mean-square displacement of an ensemble of citizens of a city from their individual homes as computed by tracking GPS location data (Makris et al. 2023a, b).

With reference to Fig. 3 we assume for now that a single traffic city artery—say freeway I-30—is a closed, one-dimensional domain where vehicles can only move within this domain as shown in Fig. 4.

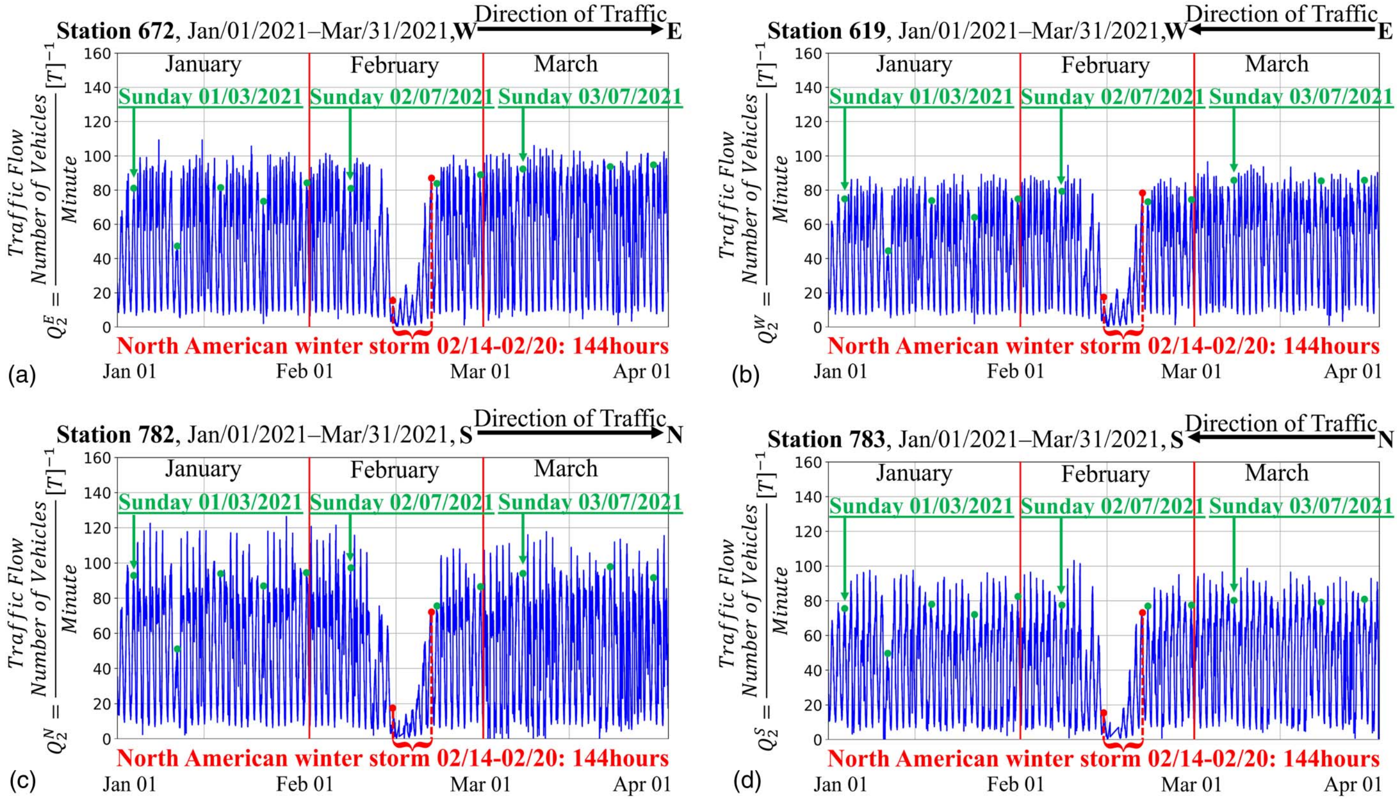

Fig. 5. Time histories of the traffic-flow Q_2^E and Q_2^W as vehicles are moving along the freeway I-30 when counted (a) at Station 672; and (b) at Station 619. Time histories of the traffic-flow Q_2^N and Q_2^S as vehicles are moving along the freeway I-35E when counted (c) at Station 782; and (d) at Station 783.

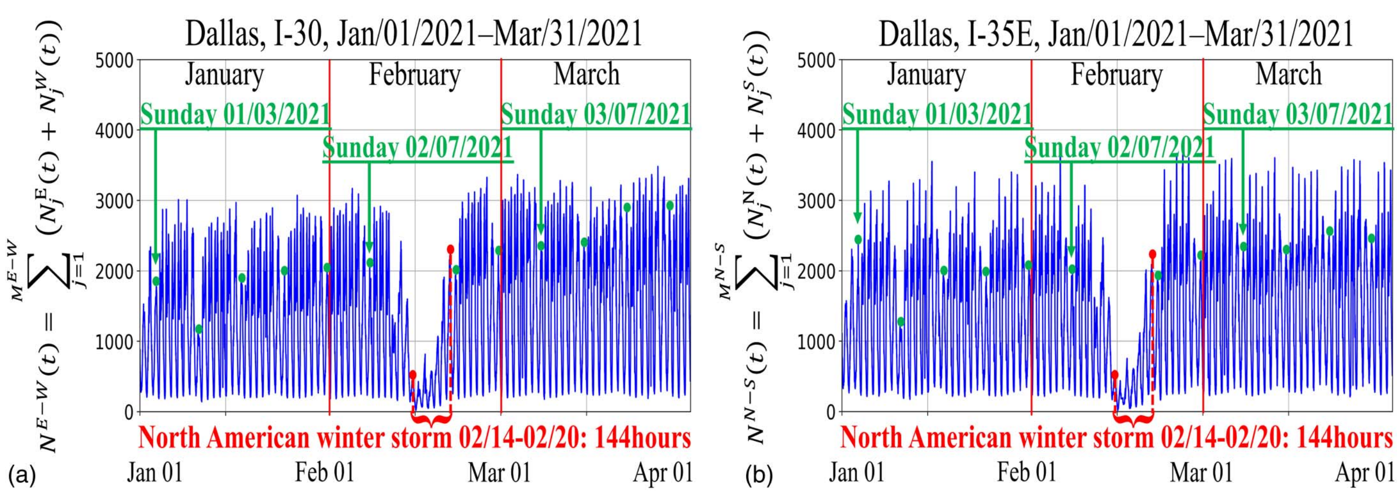

Fig. 6. Time histories of the total number of vehicles (a) $N^{E-W}(t)$ from L_W and L_E on freeway I-30; and (b) $N^{N-S}(t)$ from L_S and L_N on freeway I-35E during the first quarter of 2021. Dots upon the suppressed spikes indicate Sundays. Note the striking similarities between the time histories shown in Fig. 6 with the mean-square displacement (MSD) time histories shown in Fig. 2.

After we develop our framework of analysis, additional traffic city arteries can be added (assuming that traffic-flow data are available for these additional traffic city arteries) to obtain a more representative domain and an increasingly dependable expression of finding a given vehicle at a distance x away from the city center at time t.

Starting from a single freeway that runs east–west, the probability distribution of finding a given vehicle moving eastbound at position $x \in [L_W, L_E]$ at time t is

$$p^E(x,t) = \frac{1}{N^{E-W}(t)} \frac{N_k^E(t)}{S_k} = \frac{1}{\sum_{j=1}^{M^{E-W}} \left(N_j^E(t) + N_j^W(t)\right)} \frac{Q_k^E(t)}{v_k^E(t)} \tag{8}$$

where M^{E-W} = number of freeway segments shown in Fig. 4, index $k \in \{1, 2, \ldots, M\}$; S_k = segment that contains the given location of interest x; $N_k^E(t)$ = total number of eastbound vehicles that happen to be along segment S_k at time t; and $v_k^E(t)$ = average velocity of the eastbound vehicles along this segment, S_k.

On the other hand, the probability distribution of finding a vehicle moving westbound at position $x \in [L_E, L_W]$ at time t is

$$p^W(x,t) = \frac{1}{N^{E-W}(t)} \frac{N_k^W(t)}{S_k} = \frac{1}{\sum_{j=1}^{M^{E-W}} \left(N_j^E(t) + N_j^W(t)\right)} \frac{Q_k^W(t)}{v_k^W(t)} \tag{9}$$

where again $k \in \{1, 2, \ldots, M\}$; S_k is also the segment that contains the given location x; and $v_k^W(t)$ = average velocity of the westbound vehicle along this segment, S_k. The denominator $N^{E-W}(t)$ in Eqs. (8) and (9) is the total number of vehicles moving along the freeway from L_W to L_E at time t given by Eq. (6).

Accordingly, the probability distribution of finding a vehicle at position x, regardless of whether is moving eastbound or westbound, is

$$p^{E-W}(x,t) = p^E(x,t) + p^W(x,t) = \frac{1}{\sum_{j=1}^{M^{E-W}} (N_j^E(t) + N_j^W(t))} \left[\frac{Q_k^E(t)}{v_k^E(t)} + \frac{Q_k^W(t)}{v_k^W(t)}\right] \tag{10}$$

Clearly, the probability of finding a moving vehicle that belongs on a given freeway (domain) at time t, regardless of whether it is moving eastbound or westbound, along the entire closed domain $[L_W, L_E]$ shall be equal to 1. Accordingly

$$\int_{L_W}^{L_E} p^{E-W}(x,t)dx = \frac{1}{\sum_{j=1}^{M^{E-W}} (N_j^E(t) + N_j^W(t))} \times \sum_{k=1}^{M^{E-W}} \left(\frac{Q_k^E(t)}{v_k^E(t)} + \frac{Q_k^W(t)}{v_k^W(t)}\right) S_k \tag{11}$$

From Eqs. (4) and (5)

$$\sum_{k=1}^{M^{E-W}} \frac{Q_k^E(t)}{v_k^E(t)} S_k = \sum_{k=1}^{M^{E-W}} N_k^E(t) \quad \text{and} \quad \sum_{k=1}^{M^{E-W}} \frac{Q_k^W(t)}{v_k^W(t)} S_k = \sum_{k=1}^{M^{E-W}} N_k^W(t) \tag{12}$$

Substitution of the right-hand sides of Eq. (12) into Eq. (11) gives

$$\int_{L_W}^{L_E} p^{E-W}(x,t)dx = \frac{1}{\sum_{j=1}^{M^{E-W}} (N_j^E(t) + N_j^W(t))} \times \left[\sum_{k=1}^{M^{E-W}} N_k^E(t) + \sum_{k=1}^{M^{E-W}} N_k^W(t)\right] = 1 \tag{13}$$

Fig. 7(a) plots the traffic-flow value $Q(t)$ at $t = $ 7:00 a.m. as recorded from all recording stations along freeway I-30, while Fig. 7(b) shows the corresponding recorded average velocities as the vehicles are crossing the monitoring stations. The left column is for traffic moving from west to east, while the right column is for traffic moving from east to west. Fig. 7(c) plots the probability distribution of finding a given vehicle at position x at $t = $ 7:00 a.m. when it is moving either eastbound or westbound as given by Eqs. (8) and (9). Clearly the cumulative area under both Fig. 7(c) plots sums up to 1 as dictated by Eq. (13).

Fig. 8(a) plots the superposition of the two plots $p^{E-W}(x,t) = p^E(x,t) + p^W(x,t)$ shown in Fig. 7(c), that is, the probability distribution of finding a vehicle at position x at 7 a.m. regardless whether it moves eastbound or westbound on freeway I-30 as given by Eq. (10). Similarly Fig. 8(b) shows the probability distribution of finding a vehicle at position x at 7 a.m. regardless whether it moves northbound or southbound on freeway I-35E shown in Fig. 3(a).

Our analysis framework is generalized to estimate the probability of finding a vehicle at a distance x from the center of a city, at time t, which can move on a wider domain that consists of several freeways. For instance, in the event that a vehicle can move on both freeways $I-30 = \alpha_1$ and $I-35E = \alpha_2$, the probability distribution of finding the vehicle at a distance x from the city center is

$$p^{[E-W,N-S]}(x,t) = \frac{1}{N^{E-W}(t) + N^{N-S}(t)} \times \left[\frac{Q_k^E(t)}{v_k^E(t)} + \frac{Q_k^W(t)}{v_k^W(t)} + \frac{Q_i^N(t)}{v_i^N(t)} + \frac{Q_i^S(t)}{v_i^S(t)}\right] \tag{14}$$

where $N^{E-W}(t)$ is given by Eq. (6); and $N^{N-S}(t)$ = total number of vehicles that are moving along a north–south freeway

$$N^{N-S}(t) = \sum_{i=1}^{M^{N-S}} (N_i^N(t) + N_i^S(t)) = \sum_{i=1}^{M^{N-S}} \left(\frac{Q_i^N(t)}{v_i^N(t)} + \frac{Q_i^S(t)}{v_i^S(t)}\right) S_i \tag{15}$$

Again, the probability of finding a moving vehicle that is on freeway I-30 or I-35E at time t along their entire domain—that is $[L_W - L_E]$ for I-30 and $[L_S - L_N]$ for I-35E—shall be equal to 1 (one)

$$\int_{\text{all Segments}} p^{[E-W,N-S]}(x,t)dx = \frac{1}{N^{E-W}(t) + N^{N-S}(t)} \left[\sum_{j=1}^{M^{E-W}} \left(\frac{Q_j^E(t)}{v_j^E(t)} + \frac{Q_j^W(t)}{v_j^W(t)}\right) S_j + \sum_{i=1}^{M^{N-S}} \left(\frac{Q_i^N(t)}{v_i^N(t)} + \frac{Q_i^S(t)}{v_i^S(t)}\right) S_i\right] = 1 \tag{16}$$

given that the first summation in the right-hand side of Eq. (16) is equal to $N^{E-W}(t)$ from Eq. (6), whereas the second summation in the right-hand side of Eq. (16) is equal to $N^{N-S}(t)$ from Eq. (15).

For vehicles that their domain of motion is freeways I-30 and I-35E, Fig. 9 shows the probability distribution of finding a given vehicle at a distance x from the city center of Dallas at time $t =$ 7 a.m. [Fig. 9(a)], and $t = 9$ a.m. [Fig. 9(b)] as offered by Eq. (14). $L_+ = \max(L_E, L_N)$ is the maximum value of L_E and L_N, whereas $L_- = \min(L_W, L_S)$ is the minimum value (maximum in absolute value) for L_W and L_S. In the event that traffic-flow data are available for a number A of traffic city arteries that pass from the center of a city, as in the case of the city of Houston $(A = 3)$, as shown in Fig. 3(b), the probability of finding a given vehicle that belongs to the domain of a number A of traffic city arteries at distance x from the city center at time t is

$$p^{[1,2,\ldots,A]}(x,t) = \frac{1}{\sum_{\alpha=1}^{A} N^{\alpha}(t)} \sum_{\alpha=1}^{A} \left(\frac{Q_{k,\alpha}^1(t)}{v_{k,\alpha}^1(t)} + \frac{Q_{k,\alpha}^2(t)}{v_{k,\alpha}^2(t)}\right) \tag{17}$$

where the superscripts 1 and 2 = direction of traffic; and subscript k = segment of freeway α that contains the location x of interest. For instance, for a freeway $\alpha \in \{1, 2, \ldots, A\}$ that runs E-W, 1 = E and 2 = W.

Fig. 10(a) plots the probability $p^{[1,2,3]}(x,t)$ of finding a given vehicle at a distance x from the center of Houston, at $t = 7$ a.m. on February 1, 2021, according to Eq. (17), when considering that vehicles move in the domain that consists of freeways $\alpha_1 =$ I-10, $\alpha_2 =$ I-45, and $\alpha_3 =$ US-290 and US-288. Clearly the area under

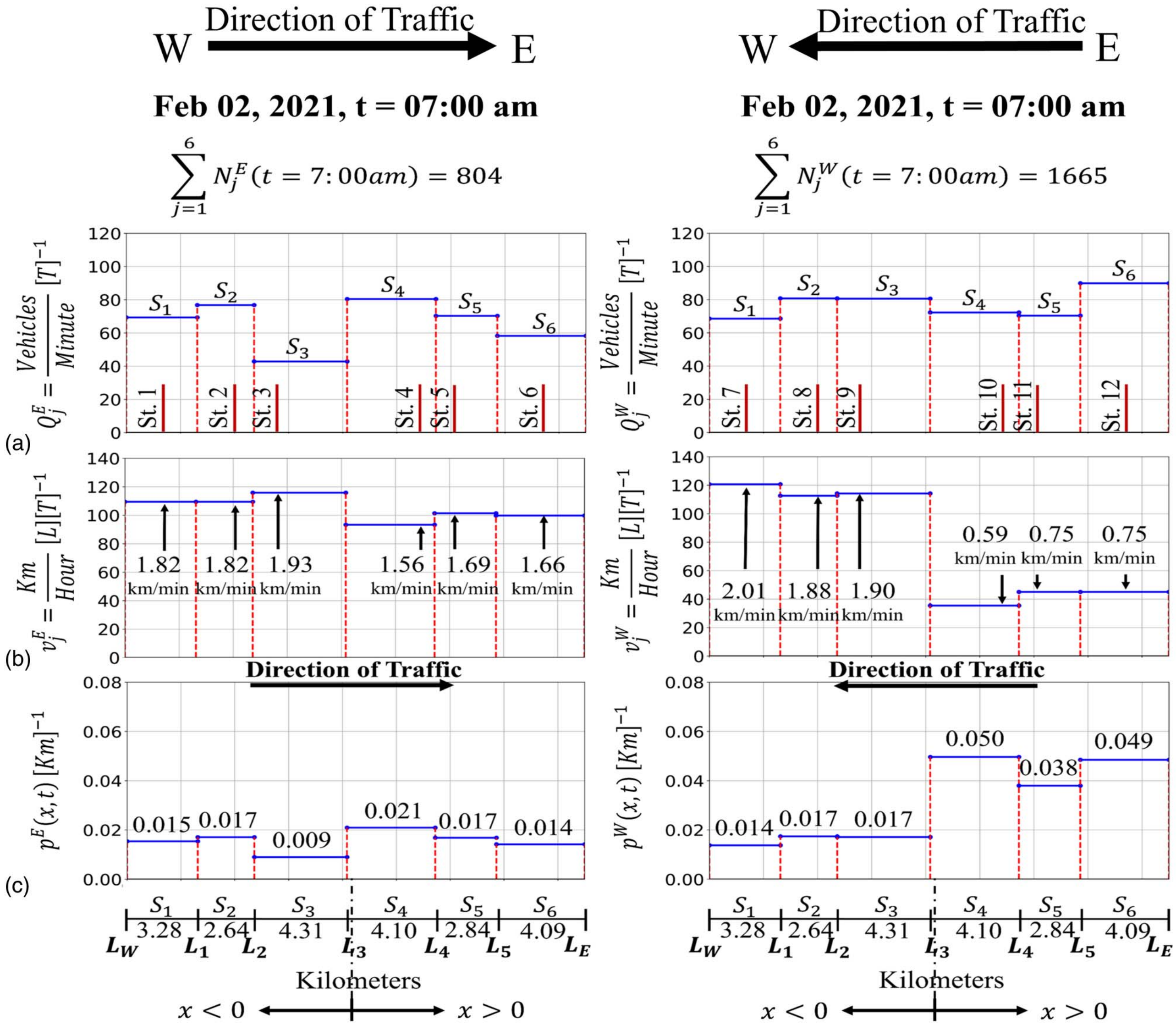

Fig. 7. (a) Traffic-flow $Q(t)$ at time $t = 7$ a.m. as recorded from all monitoring stations along freeway I-30; (b) recorded average velocities of the vehicles as they cross the monitoring stations; and (c) probability distributions, $p^E(x,t)$ and $p^W(x,t)$ offered by Eqs. (8) and (9).

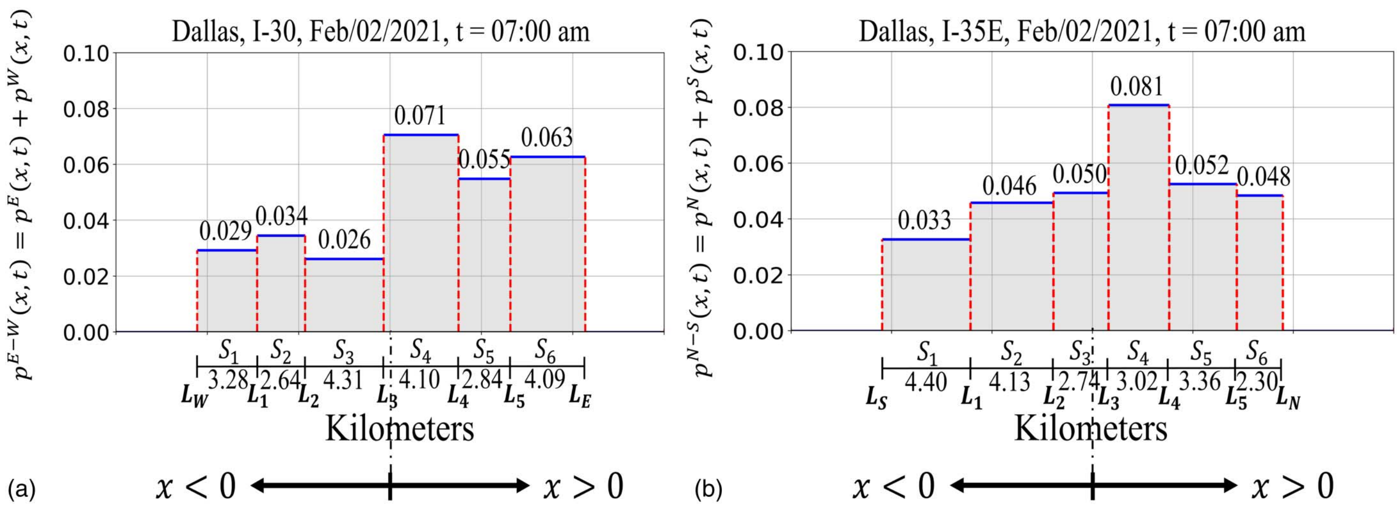

Fig. 8. (a) Superposition of the two bottom plots [$p^{E-W}(x,t) = p^E(x,t) + p^W(x,t)$] shown in Fig. 7(c), that is, the probability distribution of finding a vehicle at position x at $t = 7$ a.m. regardless whether it moves eastbound or westbound as given by Eq. (10). The gray shaded area under the curve is equal to 1. (b) Superposition of [$p^{N-S}(x,t) = p^N(x,t) + p^S(x,t)$] that is the probability distribution of finding a vehicle at position x at $t = 7$ a.m. regardless whether it moves northbound or southbound. The gray shaded area under the curve is equal to 1.

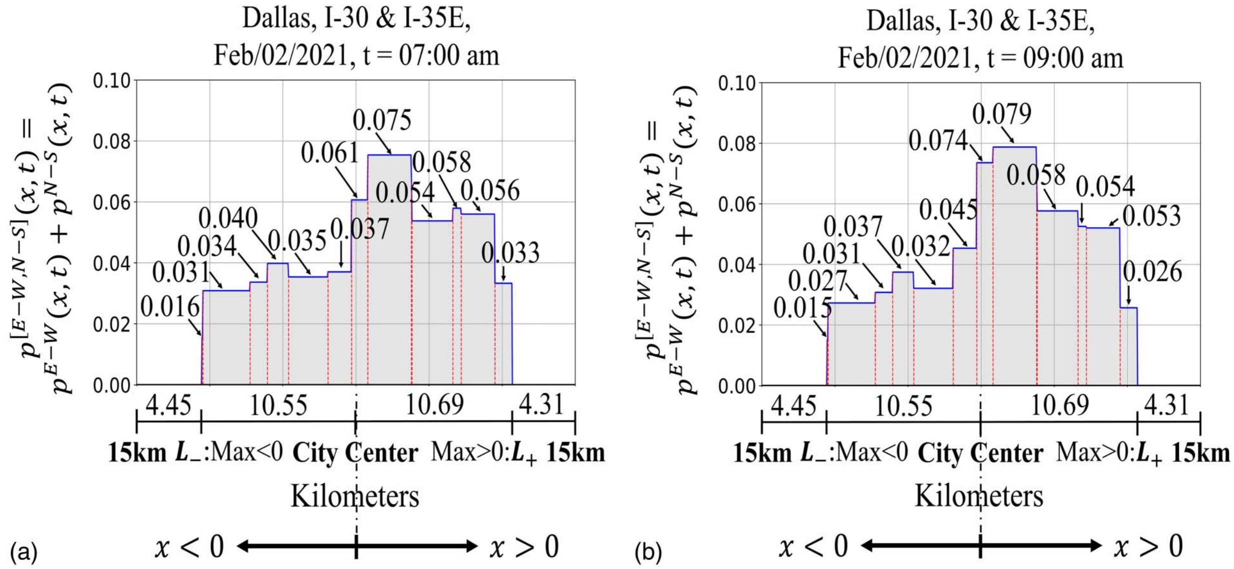

Fig. 9. Superposition of the two plots shown in Fig. 8, $p^{[E-W,N-S]}(x,t) = p^{E-W}(x,t) + p^{N-S}(x,t)$ that is, the probability distribution of finding a vehicle at position x at (a) $t = 7$ a.m.; and (b) $t = 9$ a.m. on February 2, 2021, regardless whether it moves on I-30 (E-W) or on I-35E (N-S). The gray shaded area under the curve is equal to 1.

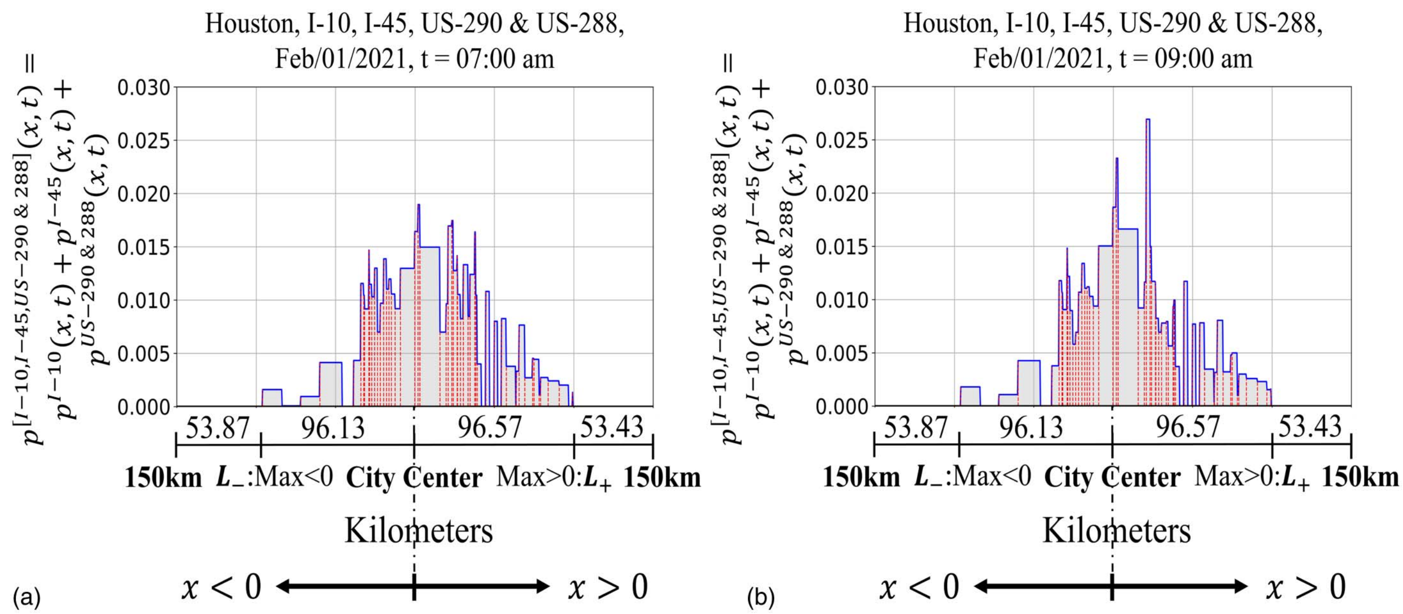

Fig. 10. Superposition of probability distribution plots for Houston area, that is, the probability distribution $p^{[1,2,3]}(x,t)$ of finding a vehicle at position x at (a) $t = 7$ a.m.; and (b) $t = 9$ a.m. on February 1, 2021 regardless whether it moves on I-10 (E-W), on I-45 (N-S) or on US-290 and US-288 (NW-SE). The gray shaded area under the curve is equal to 1.

the probability distribution shown in Fig. 10 equals to 1. Fig. 10(b) plots the corresponding probability distribution $p^{[1,2,3]}(x,t)$ of finding a given vehicle at distance x from the city center of Houston at $t = 9$ a.m. on February 1, 2021.

Figs. 9 and 10 show that as the domain, where vehicles are allowed to move contains more and more traffic city arteries, the center of the probability distribution of finding a vehicle at position x at time t shifts toward the center of the graph, since city centers are more congested with traffic moving slower.

In the interest of simplicity, we revert to the city of Dallas where we have data from only two freeways, as shown in Fig. 3(a). Fig. 11 plots the time histories of the total number of vehicles that happen to be moving in the closed domain that consists solely of freeways $\alpha_1 =$ I-30 and $\alpha_2 =$ I-35E shown in Fig. 6. This total number of vehicles, $N^{\text{I-30}}(t) + N^{\text{I-35E}}(t)$, which is the denominator of Eqs. (14), (16), and (17) for $A = 2$ when we produced Fig. 9, fluctuates with time as shown in Fig. 11, indicating that at any given time some vehicles that belong to this closed domain are parked, with the larger number of vehicles being parked at night. Accordingly, since at any given time in the closed domain that consists of freeways I-30 and I-35E shown in Fig. 3(a), some vehicles that belong to the domain are parked, a better estimate of the probability of finding a given vehicle among all vehicles that belong to the closed domain (moving and parked) at position x at time t is to replace

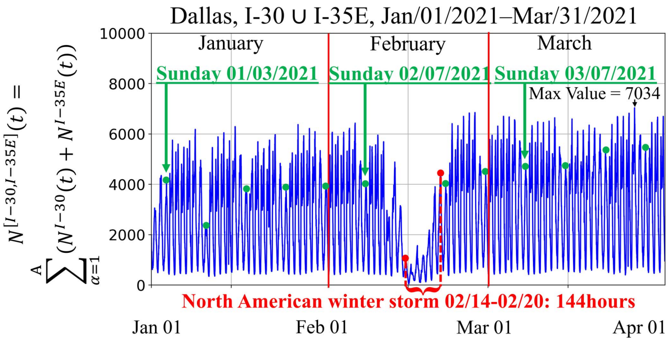

Fig. 11. Time history of the total number of vehicles that happen to be moving along both freeways I-30 and I-35E during the first quarter of 2021. Dots upon the suppressed spikes indicate Sundays.

the denominator in Eq. (17) with the maximum number of vehicles that appear within the domain over time = $\max_t \sum_{\alpha=1}^{A} N^{\alpha}(t)$. In this way Eq. (17) is revised to

$$p^{[1,2,\ldots,A]}(x,t) = \frac{1}{\max\limits_{t} \sum_{\alpha=1}^{A} N^{\alpha}(t)} \sum_{\alpha=1}^{A} \left(\frac{Q^1_{k,\alpha}(t)}{v^1_{k,\alpha}(t)} + \frac{Q^2_{k,\alpha}(t)}{v^2_{k,\alpha}(t)} \right) \tag{18}$$

Fig. 12 shows the revised probability distributions of finding a given vehicle at a distance x, from the city center of Dallas at time $t = 7$ a.m. [Fig. 12(a)] and time $t = 9$ a.m. [Fig. 12(b)] as offered by Eq. (18) in which $A = 2$. Clearly, the integral over all freeways segments of Eq. (18) is less than 1, since the stationary (parked) vehicles are not counted by the recorded stations. The advantage of Eq. (18) versus Eq. (17) is that the denominator, $\max_t \sum_{\alpha=1}^{A} N^{\alpha}(t)$, is time-independent. Upon establishing the probability density $p^{[1,2,\ldots,A]}(x,t)$ of finding a vehicle at location x at time t away from the city center, as given by Eq. (18), the mean-square displacement of a vehicle from the city center is

$$\langle x^2(t) \rangle = \int_{L_-}^{L_+} x^2 p^{[1,2,\ldots,A]}(x,t)\,dx \tag{19}$$

With reference to Fig. 12, Eq. (18) is a step-wise function, which assumes a constant value along each step that is taken out of the integral sign. Accordingly, Eq. (19) gives

$$\begin{aligned} \langle x^2(t) \rangle &= \sum_{k=1}^{S} p_k^{[1,2,\ldots,A]}(t) \int_{L_{k-1}}^{L_k} x^2 dx \\ &= \frac{1}{3} \sum_{k=1}^{S} p_k^{[1,2,\ldots,A]}(t) \left[L_k^3 - L_{k-1}^3 \right] \end{aligned} \tag{20}$$

where S = total number of steps that the probability distribution function exhibits. When $k = 1$, $L_{k-1} = L_0 = L_-$, whereas when $k = S$, $L_S = L_+$.

Fig. 13 plots with a dotted line the time history of the mean-square displacement = $\langle x^2(t) \rangle$ from the Dallas city center as results from Eq. (20), of vehicles that belong to the domain $\{\mathrm{I}-30 \cup \mathrm{I}-35\mathrm{E}\}$ during the first quarter of year 2021. Plot (a) is when the locations of L_- and L_+ are at a distance away from the first and last station, which is equal to half the distance between the first two or last two stations, respectively. Plot (b) is when the locations of L_- and L_+ are at a distance away from the first and last stations that is three times the distance between the first two or last two stations, respectively. Clearly the values of the calculated MSD = MSD = $\langle x^2(t) \rangle$ shown in Fig. 12(b) are larger, merely because the moment of area from the last term of Eq. (20) is larger. As we indicated in the discussion of Fig. 2, an analysis methodology hinges only upon the normalized expression of the calculated MSD time histories, and not on their resulting magnitudes; therefore the exact values of L_+ and L_- in Eqs. (19) and (20) are immaterial. The structure of Eq. (20) explains the striking similarities between the traffic-flow data $Q_k(t)$ shown in Fig. 5 and the mean-square displacement shown in Fig. 2 that has been computed by tracking tens of thousands of cellphone IDs. Eq. (20) dictates that the mean-square displacement of vehicles from the city center is proportional to traffic-flow data $Q(t)$ amplified by the moment of area of the maximum length of the freeway that belongs in the domain under consideration.

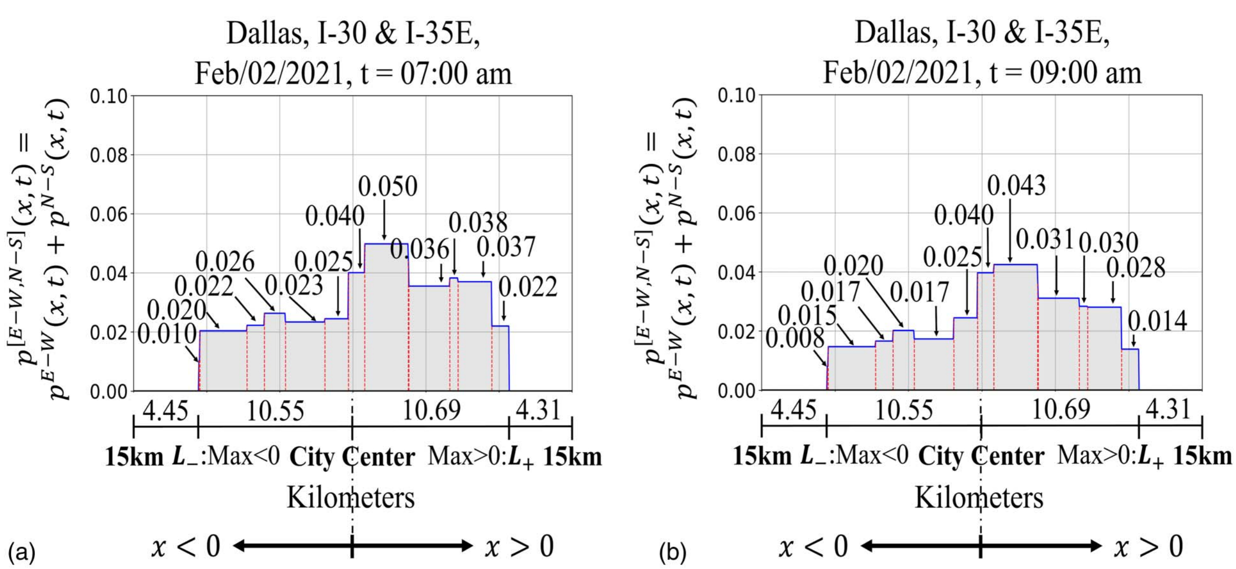

Fig. 12. Probability distributions of finding a vehicle at position x at (a) $t = 7$ a.m.; and (b) at $t = 9$ a.m. on February 1, 2021, regardless whether the vehicle moves along I-30 (E-W) or I-35E (N-S) as offered by Eq. (18).

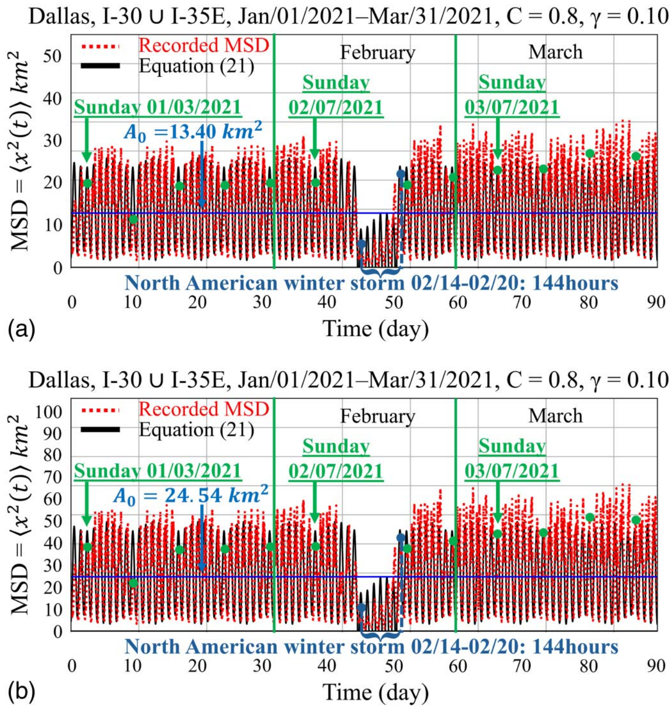

Fig. 13. Time histories of the mean-square displacement $\langle x^2(t)\rangle$ of vehicles from the Dallas city center during $Q1$, 2021. Dotted lines are for $\langle x^2(t)\rangle$ extracted from traffic-flow data given by Eq. (20). Black solid lines are for $\langle x^2(t)\rangle$ calculated from the amplitude-modulation expression given by Eq. (21). In plot (b), the distance from L_- to L_+ is larger than in plot (a).

Engineering Significance of the Mean-Square Displacement

In view of the overarching validity of Eq. (7) in the quantitative theory of Brownian motion Einstein (1905), Langevin (1908), Ornstein (1917), Landau and Lifshitz (1980), Coffey and Kalmykov (2012), Attard (2012), and Makris et al. (2023a, b) built upon the profound implications of Eq. (7) to conjecture a corresponding relation for cities

$$\langle x^2(t)\rangle = WJ(t) = A_0\left\{U(t-0) - C\left[\cos(\omega_R t) + \frac{\gamma}{2}\left(\sin\left(\frac{8}{7}\omega_R t\right) - \sin\left(\frac{6}{7}\omega_R t\right)\right)\right]\right\} \tag{21}$$

where now $\langle x^2(t)\rangle$ is the mean-square displacement of vehicles from the center of the city. The function $U(t-0)$ appearing in Eq. (21) is the unit-amplitude Heaviside step-function (Lighthill 1958), $\omega_R = 2\pi/24 = \pi/12$ rad/h is the daily frequency and parameters A_0, C, and γ are constants of the model.

The amplitude-modulation model expressed by Eq. (21) was constructed by using technique for manipulating signals in radio communications (Gray and Graham 1961; Silver 2011). Fig. 13 compares the MSD $= \langle x^2(t)\rangle$ from the city of Dallas as extracted from recorded traffic-flow data according to Eq. (20) with the predictions of the calibrated amplitude-modulation model given by Eq. (21) with $A_0 = 13.40$ km^2 [Fig. 13(a)], with $A_0 = 24.54$ km^2 [Fig. 13(b)], $C = 0.8$, and $\gamma = 0.10$ in either plot.

In view of the satisfactory performance of the analytical expression offered by Eq. (21) to capture the steady-state regime of cities under normal, operating conditions as shown in Fig. 13 for the city of Dallas, Eq. (7) dictates that the mechanical model with creep compliance (Makris et al. 2023a, b)

$$J(t) = \frac{\langle x^2(t)\rangle}{W} = \frac{\langle x^2(t)\rangle}{A_0 k} = \frac{1}{k}\left\{U(t-0) - C\left[\cos(\omega_R t) + \frac{\gamma}{2}\left(\sin\left(\frac{8}{7}\omega_R t\right) - \sin\left(\frac{6}{7}\omega_R t\right)\right)\right]\right\} \tag{22}$$

is indeed a mechanical analog for cities which predicts with fidelity their postevent regime as was shown for the city of Dallas (Makris et al. 2023a). In Eq. (22), $k = W/A_0$ is a constant with units of stiffness ($[F]/[L]$). In our analysis, natural hazards such as earthquakes, hurricanes, and winter storms, which are abrupt, finite, and system-wide, are represented mathematically with an elementary rectangular pulse of amplitude F_0 and duration T_e, which is expressed as

$$F(t) = F_0[U(t-0) - U(t-T_e)] \tag{23}$$

Other societal stressors such as pandemics and economic crises are stressing cities during larger time-scales along which the city may develop mechanisms to readjust (Meerow et al. 2016; Holling 1996). Accordingly, for such prolonged crisis that ramps up gradually and may have long tails, different loading patterns than the rectangular pulse described with Eq. (23) may be more suitable.

The creep compliance $J(t)$ (displacement history due to a unit-step force) is a time response function of a linear system. Given the linearity of the mechanical model for a city as expressed by Eq. (21) or Eq. (22), the response, $u(t)$, of the mechanical model due to a force excitation $F(t)$ is offered through the convolution integral

$$u(t) = \int_{0^-}^{t} h(t-\xi)F(\xi)d\xi \tag{24}$$

where $F(\xi)$ = time history of the acute shock—in this analysis the rectangular pulse given by Eq. (23); and $h(t)$ = impulse response function (Clough and Penzien 1970; Oppenheim and Schafer 1975; Harris and Crede 1976; Reid 1983; Makris 2021a) that is defined as the resulting displacement history, $u(t)$, due to an impulsive force input $F(t) = \delta(t-\xi)$ with $\xi < t$. Given that $\delta(t-\xi) = \mathrm{d}U(t-\xi)/\mathrm{d}t$, the impulse response function of a linear system $h(t) = \mathrm{d}J(t)/\mathrm{d}t$, where $J(t)$ is its creep compliance of the city given by Eq. (22). Accordingly, the impulse response function of the mechanical model of a city described with Eq. (22) is

$$h(t) = \frac{dJ(t)}{dt} = \frac{1}{k}\left\{\delta(t-0) + C\omega_R\left[\sin(\omega_R t) - \frac{\gamma}{2}\left(\frac{8}{7}\cos\left(\frac{8}{7}\omega_R t\right) - \frac{6}{7}\cos\left(\frac{6}{7}\omega_R t\right)\right)\right]\right\} \tag{25}$$

Upon substitution of the expression of the impulse response function given by Eq. (25) into Eq. (24) after using the forcing function $F(\xi)$ as expressed by Eq. (23), the normalized displacement response from the amplitude-modulation model when subjected to a rectangular pulse of duration T_e is (Makris et al. 2023a)

$$\frac{k}{F_0}u(t) = U(t-0) - U(t-T_e) + C\Bigg[-\cos(\omega_R t) + \cos(\omega_R(t-T_e)) - \frac{\gamma}{2}\left(\sin\left(\frac{8}{7}\omega_R t\right) - \sin\left(\frac{8}{7}\omega_R(t-T_e)\right) - \sin\left(\frac{6}{7}\omega_R t\right) + \sin\left(\frac{6}{7}\omega_R(t-T_e)\right)\right)\Bigg] \tag{26}$$

With reference to Fig. 13 [either (a) or (b)], prior to the arrival of the North American winter storm, the city of Dallas, TX, was operating under normal conditions, and its mean-square displacement $\langle x^2(t)\rangle$ of its vehicles from monitoring traffic stations is described satisfactorily with the amplitude-modulation model given by Eq. (21) and plotted at the top of Fig. 14(a) (see also Fig. 13). While Dallas was operating under normal conditions, on Sunday, February 14 $= t_0 = 0$, it was suddenly subjected to the North American winter storm, which is described with the rectangular pulse with a duration $T_e = (6\text{ days}) \times (24\text{h/day}) = 144$ hours as shown in Fig. 14(b), which is the duration reported by the media (National Oceanic and Atmospheric Administration 2021; National Weather Service 2021). The overall response, upon the city of Dallas, is subjected to the acute cold storm (postevent response), is the superposition of its steady-state response under normal operating conditions is given by Eq. (21), and its response due to the rectangular pulse is given by Eq. (26) and shown in Fig. 14(c). Accordingly, the "postevent" response of a city described with the amplitude-modulation model given by Eq. (21) is

$$kJ(t) - \frac{k}{F_0}u(t) = U(t-T_e) - C\Bigg[\cos(\omega_R(t-T_e)) + \frac{\gamma}{2}\left(\sin\left(\frac{8}{7}\omega_R(t-T_e)\right) - \sin\left(\frac{6}{7}\omega_R(t-T_e)\right)\right)\Bigg] \tag{27}$$

The left-hand side of Eq. (27) is the superposition of the response of the city under normal conditions given by Eq. (22) and its response due to the rectangular pulse given by Eq. (26).

Our main motivation for developing a mechanical model for cities as described by Eq. (21) or Eq. (22) is for estimating the recovery time of a city when struck by a natural hazard—that is, how much time the city needs to revert to its initial steady-state behavior and resume its normal pre-event activities as explained in our publications, Makris et al. (2023a, b). As an example, Fig. 14(d) shows that the predicted postevent response of the city of Dallas when the duration of excitation of the rectangular pulse is $T_e = 6$ days $= 144$ h synchronizes with the recorded postevent MSD, indicating that the city of Dallas recovered essentially immediately from the February 2021 North American winter storm. In the general case, the recovery time, T_{rec}, is the difference between T_e (duration of the rectangular pulse) and the actual duration of the natural hazard, T_{nh}, as documented by the federal and state agencies—that is, $T_{\text{rec}} = T_e - T_{\text{nh}}$. Accordingly, for the city of Dallas, when struck by the February 2021 North American winter storm, Fig. 14(d) suggests that the recovery time is essentially zero ($T_{\text{rec}} = T_e - T_{\text{nh}} = 0$).

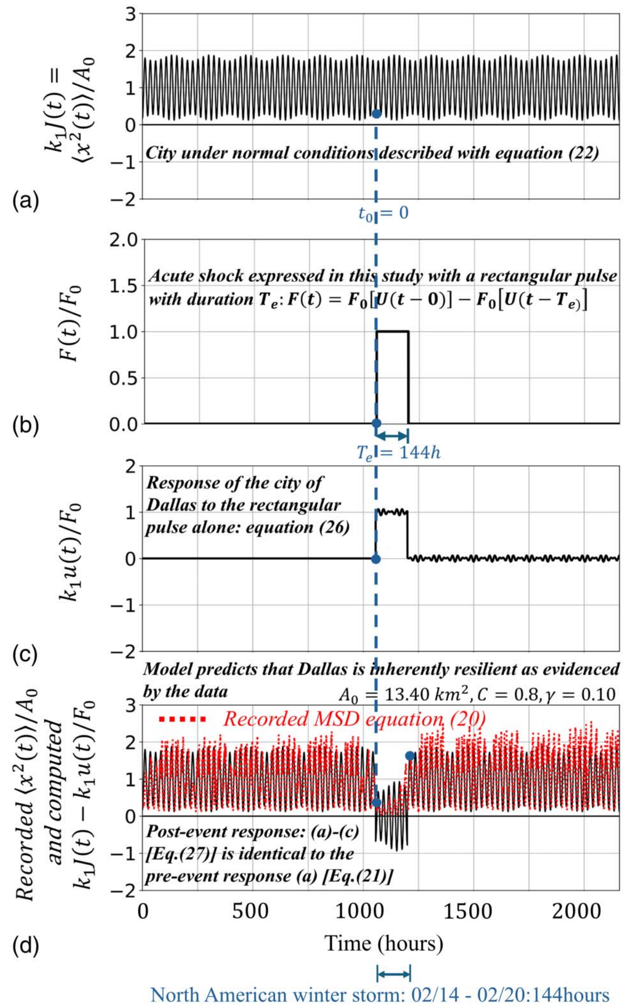

Fig. 14. (a) Normalized behavior of the city of Dallas under normal conditions as given by Eq. (22); (b) acute shock on a city expressed with a rectangular pulse with duration $T_e = 144$ h that is an integer multiple of a day = 24 h; (c) normalized response of the city of Dallas to the rectangular pulse alone with duration $T_e = 144$ h; and (d) pre- and postevent response of the city of Dallas [(a–c), solid dark lines], which is identical to the pre-event. The dotted line is the normalized recorded MSD of the city of Dallas prior, during and after the North American winter storm during the third week of February 2021 as distilled from the vehicles of the monitoring traffic station data.

Discussion

When we first developed our proposed framework of analysis by tracking GPS locations of individual cellphone IDs and then taking ensemble averages (Makris et al. 2023a, b), as indicated by Eq. (1) of the manuscript, it was evident that the resulting mean-square displacement is system-wide. In this way "traffic stresses," such as rush hours, school hours, and increased traffic from various sporting or concert events, were not captured. The work presented in this manuscript comes to complement our initial framework of analysis, since increased traffic during rush hours is encoded in the traffic-flow data shown in Fig. 7 of the manuscript and the resulting probability distributions for a single traffic city artery as shown in Fig. 8. Accordingly, in the event that a "traffic stress" from a concert or a sporting event is of interest, one should produce Fig. 7 for the specific traffic city arteries that lead to this event for the times of interest. We emphasize that the aim of our proposed framework of analysis is merely to estimate the recovery time of an entire city upon a natural hazard strikes as illustrated in Fig. 14. Accordingly, as we superimpose traffic-flow data from a number of traffic city arteries as expressed with Eq. (17) and illustrated in Fig. 10, the resulting probability distribution becomes more system-wide, and

J. Eng. Mech., 2026, 152(2): 04025098

therefore there is agreement between the time histories of ensemble averages from tracking individual IDs and the time histories from traffic-flow data (measuring the number of IDs/time that pass from a given location).

Conclusions

We have developed an analysis framework for the quantification of urban resilience to natural hazards in which the resilience of the living network of the citizens of a city is encoded by processing traffic-flow data (number of vehicles per time) recorded at various locations along major traffic city arteries.

Upon superimposing traffic-flow data from various traffic city arteries, we evaluate the probability density, $p(x,t)$ of finding a given vehicle at a distance x from the city center at time t, and we calculate its second moment, $\langle x^2(t)\rangle = \int_{L_-}^{L_+} x^2 p(x,t)dx$. Our study concentrates on a "single-state equilibrium" that is the response history of the mean-square displacement = $\langle x^2(t)\rangle$ (MSD) of vehicles from the city center. The shape of the MSD = $\langle x^2(t)\rangle$ time histories of vehicles computed in this study from traffic-flow data exhibits striking similarities with the MSD time histories computed by tracking GPS locations from individual cellphone users. Accordingly, this study, which uses an entirely different type of data (traffic-flow data) confirms our previous finding (that emerged from cellphone GPS location data) that large American cities with average to high population densities, following a natural hazard, revert immediately to their initial steady-state behavior and resume the normal, pre-event activities. In conclusion, our analysis framework for the quantification of urban resilience to natural hazards from human mobility data concludes that large American cities exhibit an inherent resilience.

Data Availability Statement

The traffic-flow data used in this study were obtained from State Departments of Transportation and regional transportation authorities, including the Texas Department of Transportation (TxDOT), the North Central Texas Council of Governments (NCTCOG), and the Texas A&M Transportation Institute (TTI) (North Central Texas Council of Governments 2025; Texas A&M Transportation Institute 2025). These agencies monitor vehicular traffic along major urban freeways by collecting vehicle count data across time at numerous fixed stations. The datasets used in this manuscript specifically include data collected along major corridors in Dallas and Houston, TX, such as I–30, I–35E, I–10, I–45, US Highway 288, and US Highway 290. All data, models, or code that support the findings of this study are available from the corresponding author upon reasonable request.

Acknowledgments

The authors are gratefull to F. Torres from the North Central Texas Council of Governments (NCTCOG) in Dallas, TX, for assistance in facilitating the first author's access to traffic data from the Dallas region and for introducing M. Vickich from the Texas A&M Transportation Institute (TTI), whose collaboration provided access to additional traffic data from the Houston metropolitan region (North Central Texas Council of Governments 2025; Texas A&M Transportation Institute 2025). Data analysis was performed on the ManeFrame III (M3) and SuperPOD high-performance computing (HPC) cluster. Computational resources for this research were provided by SMU's O'Donnell Data Science and Research Computing Institute.

Author Contributions

Georgios Chatzikyriakidis: Data curation; Investigation; Software; Validation; Visualization; Writing – review and editing. Nicos Makris: Conceptualization; Formal analysis; Investigation; Methodology; Project administration; Supervision; Visualization; Writing – original draft; Writing – review and editing. Tue Vu: Data curation; Software; Validation.

References

Achillopoulou, D. V., S. A. Mitoulis, S. A. Argyroudis, and Y. Wang. 2020. "Monitoring of transport infrastructure exposed to multiple hazards: A roadmap for building resilience." *Sci. Total Environ.* 746 (Dec): 141001. https://doi.org/10.1016/j.scitotenv.2020.141001.

Attard, P. 2012. *Non-equilibrium thermodynamics and statistical mechanics: Foundations and applications*. New York: Oxford University Press.

Bettencourt, L., and G. West. 2010. "A unified theory of urban living." *Nature* 467 (7318): 912–913. https://doi.org/10.1038/467912a.

Bettencourt, L. M. A. 2013. "The origins of scaling in cities." *Science* 340 (6139): 1438–1441. https://doi.org/10.1126/science.1235823.

Blagojević, N., F. Hefti, J. Henken, M. Didier, and B. Stojadinović. 2023. "Quantifying disaster resilience of a community with interdependent civil infrastructure systems." *Struct. Infrastruct. Eng.* 19 (12): 1696–1710. https://doi.org/10.1080/15732479.2022.2052912.

Bruneau, M., et al. 2003. "A framework to quantitatively assess and enhance the seismic resilience of communities." *Earthquake Spectra* 19 (4): 733–752. https://doi.org/10.1193/1.1623497.

Cassottana, B., L. Shen, and L. C. Tang. 2019. "Modeling the recovery process: A key dimension of resilience." *Reliab. Eng. Syst. Saf.* 190 (Oct): 106528. https://doi.org/10.1016/j.ress.2019.106528.

Chatzikyriakidis, G., N. Makris, and T. Vu. 2026. "Quantification of community resilience to natural hazards by tracking cell-phone GPS location data." *Reliab. Eng. Syst. Saf.* 266 (Sep): 111738. https://doi.org/10.1016/j.ress.2025.111738.

Clough, R. W., and J. Penzien. 1970. *Dynamics of structures*. New York: McGraw-Hill.

Coffey, W., and Y. P. Kalmykov. 2012. Vol. 27 of *The Langevin equation: With applications to stochastic problems in physics, chemistry and electrical engineering*. Singapore: World Scientific.

Cruz, S. S., J. P. T. A. Costa, S. Á. de Sousa, and P. Pinho. 2013. "Urban resilience and spatial dynamics." In *Resilience thinking in urban planning*, 53–69. Dordrecht, Netherlands: Springer.

Dalziell, E., and A. Nicholson. 2001. "Risk and impact of natural hazards on a road network." *J. Transp. Eng.* 127 (2): 159–166. https://doi.org/10.1061/(ASCE)0733-947X(2001)127:2(159).

Da Silva, J., S. Kernaghan, and A. Luque. 2012. "A systems approach to meeting the challenges of urban climate change." *Int. J. Urban Sustainable Dev.* 4 (2): 125–145. https://doi.org/10.1080/19463138.2012.718279.

Einstein, A. 1905. "Über die von der molekularkinetischen Theorie der Wärme geforderte Bewegung von in ruhenden Flüssigkeiten suspendierten Teilchen." *Ann. Phys.* 322 (8): 549–560. https://doi.org/10.1002/andp.19053220806.

Ganin, A. A., E. Massaro, A. Gutfraind, N. Steen, J. M. Keisler, A. Kott, R. Mangoubi, and I. Linkov. 2016. "Operational resilience: Concepts, design and analysis." *Sci. Rep.* 6 (1): 1–12. https://doi.org/10.1038/srep19540.

Gittes, F., B. Schnurr, P. D. Olmsted, F. C. MacKintosh, and C. F. Schmidt. 1997. "Microscopic viscoelasticity: Shear moduli of soft materials determined from thermal fluctuations." *Phys. Rev. Lett.* 79 (17): 3286. https://doi.org/10.1103/PhysRevLett.79.3286.

Godschalk, D. R. 2003. "Urban hazard mitigation: Creating resilient cities." *Nat. Hazard. Rev.* 4 (3): 136–143. https://doi.org/10.1061/(ASCE)1527-6988(2003)4:3(136).

Gray, L., and R. Graham. 1961. *Radio transmitters*. New York: McGraw-Hill.

Harris, C. M., and C. E. Crede. 1976. *Shock and vibration handbook*. New York: McGraw-Hill.

Henry, D., and J. E. Ramirez-Marquez. 2012. "Generic metrics and quantitative approaches for system resilience as a function of time." *Reliab. Eng. Syst. Saf.* 99 (Mar): 114–122. https://doi.org/10.1016/j.ress.2011.09.002.

Holling, C. S. 1973. "Resilience and stability of ecological systems." *Annu. Rev. Ecol. Evol. Syst.* 4 (Nov): 1–23. https://doi.org/10.1146/annurev.es.04.110173.000245.

Holling, C. S. 1996. "Engineering resilience versus ecological resilience." In *Engineering within ecological constraints*, 31–44. Washington, DC: National Academies Press.

Jabareen, Y. 2013. "Planning the resilient city: Concepts and strategies for coping with climate change and environmental risk." *Cities* 31 (Apr): 220–229. https://doi.org/10.1016/j.cities.2012.05.004.

Jindal, T., P. Giridhar, L.-A. Tang, J. Li, and J. Han. 2013. "Spatiotemporal periodical pattern mining in traffic data." In *Proc., 2nd ACM SIGKDD Int. Workshop on Urban Computing*, 1–8. New York: Association for Computing Machinery.

Landau, L. D., and E. M. Lifshitz. 1980. "Statistical physics." In Vol. 5 of *Course of theoretical physics*. Oxford, UK: Pergamon Press.

Langevin, P. 1908. "Sur la théorie du mouvement Brownien." *C. R. Acad. Sci.* 146: 530–533.

Lhomme, S., D. Serre, Y. Diab, and R. Laganier. 2013. "Urban technical networks resilience assessment." In *Resilience urban risk management*, 109–117. Boca Raton, FL: CRC Press.

Li, T., S. Kheifets, D. Medellin, and M. G. Raizen. 2010. "Measurement of the instantaneous velocity of a Brownian particle." *Science* 328 (5986): 1673–1675. https://doi.org/10.1126/science.1189403.

Li, T., and M. G. Raizen. 2013. "Brownian motion at short time scales." *Ann. Phys.* 525 (4): 281–295. https://doi.org/10.1002/andp.201200232.

Lighthill, M. J. 1958. *An introduction to Fourier analysis and generalised functions*. Cambridge, UK: Cambridge University Press.

Linkov, I., et al. 2014. "Changing the resilience paradigm." *Nat. Clim. Change* 4 (6): 407–409. https://doi.org/10.1038/nclimate2227.

Makris, N. 2020. "Viscous-viscoelastic correspondence principle for Brownian motion." *Phys. Rev. E* 101 (5): 052139. https://doi.org/10.1103/PhysRevE.101.052139.

Makris, N. 2021a. "Impulse response function for Brownian motion." *Soft Matter* 17 (21): 5410–5426. https://doi.org/10.1039/D1SM00380A.

Makris, N. 2021b. "A rheological analog for Brownian motion with hydrodynamic memory." *Phys. Fluids* 33 (7): 072014. https://doi.org/10.1063/5.0059452.

Makris, N., G. Moghimi, E. Godat, and T. Vu. 2023a. "Mechanical analogue for cities." *R. Soc. Open Sci.* 10 (3): 220943. https://doi.org/10.1098/rsos.220943.

Makris, N., T. Vu, G. Moghimi, G. Chatzikyriakidis, and E. Godat. 2023b. "Characterization of the inherent resilience of large cities to natural hazards." *J. Eng. Mech.* 149 (10): 04023076. https://doi.org/10.1061/JENMDT.EMENG-7102.

Mason, T. G., K. Ganesan, J. H. van Zanten, D. Wirtz, and S. C. Kuo. 1997. "Particle tracking microrheology of complex fluids." *Phys. Rev. Lett.* 79 (17): 3282. https://doi.org/10.1103/PhysRevLett.79.3282.

Mason, T. G., and D. A. Weitz. 1995. "Optical measurements of frequency-dependent linear viscoelastic moduli of complex fluids." *Phys. Rev. Lett.* 74 (7): 1250. https://doi.org/10.1103/PhysRevLett.74.1250.

Meerow, S., J. P. Newell, and M. Stults. 2016. "Defining urban resilience: A review." *Landscape Urban Plann.* 147 (Mar): 38–49. https://doi.org/10.1016/j.landurbplan.2015.11.011.

Min, W., and L. Wynter. 2011. "Real-time road traffic prediction with spatio-temporal correlations." *Transp. Res. Part C Emerging Technol.* 19 (4): 606–616. https://doi.org/10.1016/j.trc.2010.10.002.

National Oceanic and Atmospheric Administration. 2021. "Historic winter storm and arctic outbreak." Accessed June 4, 2024. https://www.weather.gov/fwd/Feb-2021-WinterEvent.

National Weather Service. 2021. "North American winter storm in Dallas." Accessed February 21, 2021. https://www.weather.gov/fwd/Feb-2021-WinterEvent.

North Central Texas Council of Governments. 2025. "Traffic count database system: Regional traffic volumes dataset." Accessed March 7, 2025. https://www.nctcog.org/.

Oppenheim, A. V., and R. W. Schafer. 1975. *Digital signal processing*. Englewood Cliffs, NJ: Prentice-Hall.

Ornstein, L. S. 1917. "On the brownian motion." In Vol. 21 of *Proc., Huygens Institute-Royal Netherlands Academy of Arts and Sciences*, 96–108. Amsterdam, Netherlands: Royal Netherlands Academy of Arts and Sciences.

Palmer, A., J. Xu, and D. Wirtz. 1998. "High-frequency viscoelasticity of crosslinked actin filament networks measured by diffusing wave spectroscopy." *Rheol. Acta* 37 (2): 97–106. https://doi.org/10.1007/s003970050095.

Qiang, Y., and J. Xu. 2020. "Empirical assessment of road network resilience in natural hazards using crowdsourced traffic data." *Int. J. Geogr. Inf. Sci.* 34 (12): 2434–2450. https://doi.org/10.1080/13658816.2019.1694681.

Reid, J. G. 1983. *Linear system fundamentals: Continuous and discrete, classic and modern*. New York: McGraw-Hill.

Roh, H.-J., S. Sharma, and P. K. Sahu. 2016. "Modeling snow and cold effects for classified highway traffic volumes." *KSCE J. Civ. Eng.* 20 (4): 1514–1525. https://doi.org/10.1007/s12205-015-0236-0.

Schnurr, B., F. Gittes, F. C. MacKintosh, and C. F. Schmidt. 1997. "Determining microscopic viscoelasticity in flexible and semiflexible polymer networks from thermal fluctuations." *Macromolecules* 30 (25): 7781–7792. https://doi.org/10.1021/ma970555n.

Shi, Q., and M. Abdel-Aty. 2015. "Big Data applications in real-time traffic operation and safety monitoring and improvement on urban expressways." *Transp. Res. Part C Emerging Technol.* 58 (Sep): 380–394. https://doi.org/10.1016/j.trc.2015.02.022.

Silver, H. W. 2011. *The ARRL handbook for radio communications*. Newington, CT: American Radio Relay League.

Texas A&M Transportation Institute. 2025. "Traffic count database system: Regional traffic volumes dataset." Accessed March 7, 2025. https://tti.tamu.edu/.

Uhlenbeck, G. E., and L. S. Ornstein. 1930. "On the theory of the Brownian motion." *Phys. Rev.* 36 (5): 823. https://doi.org/10.1103/PhysRev.36.823.

Wang, M. C., and G. E. Uhlenbeck. 1945. "On the theory of the Brownian motion II." *Rev. Mod. Phys.* 17 (2–3): 323. https://doi.org/10.1103/RevModPhys.17.323.

Yuan, H., and G. Li. 2021. "A survey of traffic prediction: From spatio-temporal data to intelligent transportation." *Data Sci. Eng.* 6 (1): 63–85. https://doi.org/10.1007/s41019-020-00151-z.